Mitigation of loss within a molecular Stark decelerator

B.C. Sawyer[1,a], B.K. Stuhl[1], B.L. Lev[1,b], J. Ye[1], and E.R. Hudson[2]

[1] JILA, National Institute of Standards and Technology and University of Colorado Department of Physics, University of Colorado, Boulder, CO 80309-0440, USA

[2] Department of Physics, Yale University, New Haven, CT 06520, USA

Abstract. The transverse motion inside a Stark decelerator plays a large role in the total efficiency of deceleration. We differentiate between two separate regimes of molecule loss during the slowing process. The first mechanism involves distributed loss due to coupling of transverse and longitudinal motion, while the second is a result of the rapid decrease of the molecular velocity within the final few stages. In this work, we describe these effects and present means for overcoming them. Solutions based on modified switching time sequences with the existing decelerator geometry lead to a large gain of stable molecules in the intermediate velocity regime, but fail to address the loss at very low final velocities. We propose a new decelerator design, the quadrupole-guiding decelerator, which eliminates distributed loss due to transverse/longitudinal couplings throughout the slowing process and also exhibits gain over normal deceleration to the lowest velocities.

PACS. 37.10.Mn Slowing and cooling of molecules – 37.20.+j Atomic and molecular beam sources and techniques – 37.90.+j Other topics in mechanical control of atoms, molecules, and ions

1 Introduction

Recent development of cold polar-molecule sources promises to reveal many interesting, and hitherto unexplored, molecular interaction dynamics. The permanent electric dipole moment possessed by polar molecules provides a new type of interaction in the ultracold environment. This electric dipole-dipole interaction (and control over it) should give rise to unique physics and chemistry including novel cold-collision dynamics [1,2] and quantum information processing [3].

To date, cold polar-molecule samples have been produced most successfully via three different mechanisms: buffer gas cooling [4,12]; photo- and magneto-association [5–8]; and Stark deceleration [9]. Buffer gas cooling achieves temperatures below 1 K through thermalization of molecules with a He buffer. This technique produces relatively large densities (10^8 cm^{-3}) of polar ground-state molecules. However, cooling below ∼100 mK has not yet been achieved because the He buffer gas has not been removed quickly enough for evaporative cooling [12]. Photoassociation achieves the lowest molecular temperatures of these techniques (∼100 μK), but is limited to molecules whose atomic constituents are amenable to laser-cooling. Furthermore, molecules in their ground

vibrational state are not readily produced, yielding species with relatively small effective electric dipoles, although this problem can be overcome with more sophisticated laser control techniques [6,14]. Stark deceleration exists as an alternative to these methods as the technique employs well-characterized supersonic beam methods [15] to produce large densities of ground state polar molecules ($\sim 10^9$ cm^{-3}), albeit at high packet velocities. One limitation of this technique for trapping of decelerated molecules is an observed drastic loss of slowed molecules at very low mean velocities in both our own group's work and the Berlin group of Meijer [16]. We address this problem in this article.

As the leading method for producing cold samples of chemically interesting polar molecules, Stark deceleration has generated cold samples of CO [9], ND$_3$ [17], OH [18–21], YbF [22], H$_2$CO [2], NH [23], and SO$_2$ [13,24], leading to the trapping of ND$_3$ [17], OH [21,25], NH [10], and CO [11]. Given the importance of Stark deceleration to the study of cold molecules, it is crucial that the technique be refined to achieve maximum deceleration efficiency. In this work, we provide a detailed description of processes that limit the efficiency of current decelerators and propose methods for overcoming them. We propose possible solutions to the parametric transverse/longitudinal coupling loss originally highlighted in reference [26], as well as elucidate a new loss mechanism unique to producing the slowest molecules. We restrict

[a] e-mail: sawyerbc@colorado.edu
[b] *Present address*: Department of Physics, University of Illinois, Urbana, IL 61801-3080, USA

the described simulations and theory to Stark decelerated, ground-state OH radicals, as the supporting experimental data was taken with this molecular species. However, the loss mechanisms described herein are not specific to OH, and represent a general limitation of current Stark decelerators. This reduces the efficiency of Stark decelerators for trapping cold polar molecules.

This article is organized as follows. Section 2 describes the mechanisms responsible for molecular loss at low velocities. Sections 3 and 4 present methods of producing molecular packets at intermediate velocities (>100 m/s) without the distributed transverse/longitudinal coupling losses of reference [26]. However, these methods exacerbate the problem of low-velocity loss. Therefore, we propose a new decelerator design in Section 5 that exhibits gain over conventional Stark deceleration to velocities as low as 14 m/s.

2 Loss at low velocities

In references [20,27], the assumption is made that all motion parallel and transverse to the decelerator axis is stable up to some maximum excursion velocity and position from the beam center, enabling the derivation of an analytical solution to predict stable-molecule phase-space area. However, there are several important instances where the assumptions of this model become invalid. In the case of very slow molecules (<50 m/s)[1], we identify two distinct phenomena leading to reduced decelerator efficiency at the final deceleration stages: transverse overfocusing and longitudinal reflection. Transverse overfocusing occurs when the decelerated molecules' speed becomes so low that the decelerating electrodes focus the molecules too tightly (transversely) and they either make contact with the electrodes or are strongly dispersed upon exiting the decelerator. Longer decelerators tend to exacerbate this effect due to the fact that molecules can travel at low speeds for many stages. Nonetheless, there are several motivating factors for constructing a longer decelerator. First, longer decelerators allow less energy per stage to be removed and consequently lead to larger longitudinal phase-space acceptance. Second, a longer decelerator may allow deceleration of molecules possessing an unfavorable Stark shift to mass ratio. We will discuss critical issues for use of such long decelerators for slow molecule production.

A second low-velocity effect, which we have denoted "longitudinal reflection", is a direct result of the spatial inhomogeneity of the electric field at the final deceleration stage. As highlighted in the context of transverse guidance in reference [26], the longitudinal potential is largest for those molecules passing — in the transverse dimension — nearest to the decelerator rods. However, the decelerator switching sequence is generally only synchronous

---

[1] This lower velocity limit depends on the molecule of interest as well as decelerator electrode geometry. In general, we expect this velocity limit to scale as $\sqrt{\mu/m}$, where μ is the effective electric dipole moment and m is the mass of the given molecule.
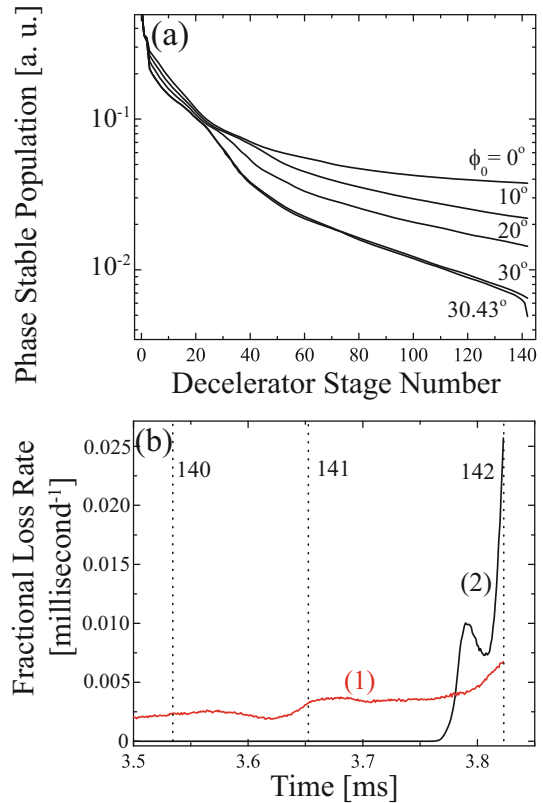
Fig. 1. (Color online) (a) Simulations of the phase-stable molecule number as a function of stage number in our 142-stage decelerator. Note the dramatic decrease in number in the last several stages for $\phi_0 = 30.43°$. This decrease is due to transverse overfocusing and longitudinal reflection of these slow (14 m/s) molecules. (b) Simulated transverse (trace 1) and longitudinal (trace 2) fractional loss rates as a function of time within the final three stages at $\phi_0 = 30.43°$. The vertical dashed lines denote the times of the given stage switches.

to a molecule on-axis traveling at the mean speed of the packet. As a result, when the mean longitudinal kinetic energy of the slowed packet becomes comparable to the Stark potential barrier at the last stage, molecules off-axis can be stopped or reflected, resulting in a spatial filtering effect. Furthermore, the longitudinal velocity spread of the molecular packet at the final stage, if larger than the final mean velocity, can lead to reflection of the slowest portion of the packet. It is important that the phenomena of overfocusing and longitudinal reflection be addressed since molecule traps fed by Stark decelerators require slow packets for efficient loading.

To illustrate these low-velocity effects, the number of phase-stable molecules predicted by three-dimensional (3D) Monte Carlo simulation is shown in Figure 1a as a function of stage number for increasing phase angle. All Monte Carlo simulation results presented in this article are based on three-dimensional models. The quoted phase-stable molecule number is determined at each time step by counting the number of molecules within the instantaneous three-dimensional spatial acceptance defined relative to the synchronous molecule. Quasi-stable molecules

— those that do not remain in the acceptance volume for the full slowing sequence — can initially lead to an over-estimate of the stable molecule number. However, we observe that such molecules exit the decelerator within the first 40 stages, therefore we reserve comparisons between deceleration schemes to the region beyond stage 40. We define the deceleration phase angle, ϕ_0, exactly as in previous publications, where $\phi_0 = (z/L)180°$ [20]. The length of one slowing stage is given by L (5.5 mm for our machine), while the molecule position between successive stages is denoted as z. We define $z = 0$ to be exactly between two slowing stages, therefore, $\phi_0 = 0°$ (bunching) yields no net deceleration. Phase angles satisfying $0° < \phi_0 < 90°$ lead to deceleration of the molecular packet, while the maximum energy is removed for $\phi_0 = 90°$. The 3D simulation results displayed in Figure 1a include both longitudinal and transverse effects. The molecules have an initial velocity ($v_{initial}$) of 380 m/s, corresponding to the mean velocity of a molecular pulse created via supersonic expansion in Xe. All simulations and experimental data hereafter possess this $v_{initial}$ unless otherwise noted.

As expected, a higher phase angle leads to a smaller number of decelerated molecules. However, there is a sharp loss of molecules in the last several deceleration stages for the highest phase of $\phi_0 = 30.43°$. This value of ϕ_0 produces a packet possessing a final velocity (v_{final}) of 14 m/s. This loss is attributed to transverse overfocusing and longitudinal reflection. These distinct effects are illustrated in Figure 1b, which displays the transverse (trace 1) and longitudinal (trace 2) fractional loss rate of molecules traversing the final three slowing stages at $\phi_0 = 30.43°$, $v_{final} = 14$ m/s. The switching time for each stage is denoted by a vertical dashed line, which is labeled by the corresponding stage number. Longitudinal reflection of molecules is clearly the dominant loss mechanism for the lowest final velocity shown in Figure 1a. Nonetheless, there also exists a non-negligible rise in transverse losses at the final stage. That is, because the molecular beam is moving very slowly in the last few deceleration stages, the transverse guiding fields of the decelerator electrodes have a greater focusing effect on the molecules (see Eq. (3) of Ref. [19]) and focus the molecules so tightly that they collide with a deceleration stage and are lost. In the case of our decelerator, this leads to loss of 20% of the decelerated molecule number between $\phi_0 = 30°$ (50 m/s) and $\phi_0 = 30.43°$ (14 m/s). Such a dramatic loss is not predicted by analytical theory, as the stable phase-space area decreases by <1% over this range of ϕ_0. This number is calculated directly after the decelerator is switched-off and is thus an upper bound, since experiments employing these cold molecules require them to travel out of the decelerator where transverse spread can lead to dramatic loss of molecule number.

Experimental evidence of this sudden decrease in molecule number at very low velocities is given in Figure 2, which displays data from time-of-flight (ToF) measurements along with corresponding Monte Carlo simulation results at various phase angles. The decelerated OH molecules are in the weak-field seeking $|F = 2, m_F = \pm 2,$
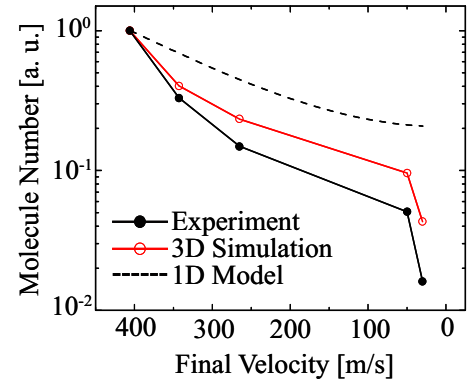

Fig. 2. (Color online) Experimental (dots) and Monte Carlo simulation (open circles) results for total molecule number as a function of final velocity. The dashed curve is the expected decelerator efficiency calculated from the one-dimensional (1D) theoretical model of reference [20].

$-\rangle$ state. The first two quantum numbers of the state denote its hyperfine components, while the third number indicates the parity of the state in the absence of electric fields. The total detected and simulated molecule numbers are plotted in Figure 2 as a function of final velocity, along with the theoretically expected decelerator efficiency (dashed line) [20]. Note that the sudden population decrease in both simulation and experimental results is not reflected in the one-dimensional theoretical model, which does not account for the transverse dynamics or field inhomogeneities that cause such behavior. This effect is detrimental to the production of dense samples of cold molecules. The difference between experiment and 3D simulation in Figure 2 is indicative of an inability to account for imperfections in decelerator construction. At low velocities, we observe smaller longitudinal velocity widths than predicted by simulation. Small errors in simulated detection aperture also have larger effects as final speed is reduced. Nonetheless, the experimentally observed dramatic molecule loss is reproduced by 3D simulation.

To remove the overfocusing effect at low velocities, the transverse focusing of the last several decelerator stages needs to be reduced. Different types of transverse focusing elements may be inserted into the deceleration beam line to compensate for this phenomenon. This idea is discussed in detail in Sections 4 and 5. We note that the proposed solutions, while successful in addressing the detrimental longitudinal/transverse coupling effects, do not mitigate the problem of longitudinal reflection at low velocities.

3 Distributed loss

As noted in previous work [13,25,26], coupling between transverse and longitudinal motion throughout the deceleration sequence invalidates the assumptions made for 1D simulations in references [20,27], thereby necessitating 3D Monte Carlo simulations. The fact that the transverse guidance of the molecular beam comes from the same electrodes that provide the deceleration means that the
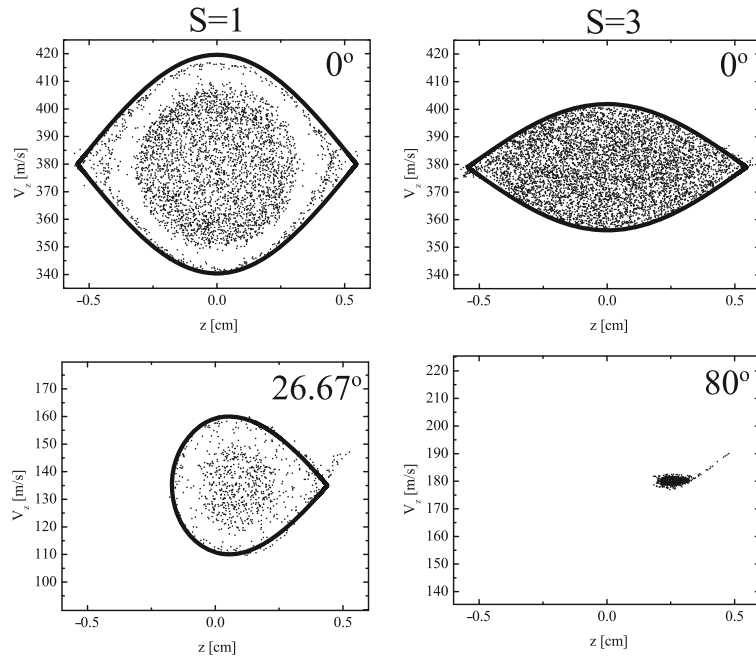
Fig. 3. Monte Carlo simulation results for the longitudinal phase space of decelerated molecules. The left column shows $\phi_0 = 0°$ and $26.67°$ for $S = 1$ slowing, while the right column shows $\phi_0 = 0°$ and $80°$ for $S = 3$ deceleration. The factor of three between $S = 1$ and $S = 3$ phase angles ensures that molecules have roughly the same final velocities. The observed velocity difference at the higher phase angle occurs because the 142 stages of our slower is not a multiple of three. Note that, although the $S = 3$ phase plot is more densely populated than that of $S = 1$ at $\phi_0 = 0°$, its phase-space acceptance decreases dramatically relative to $S = 1$ at the lowest velocities. All plots are generated using an identical initial number of molecules, and therefore the density of points is meaningful for comparison.

longitudinal and transverse motions are necessarily coupled. While this phenomenon is well understood in the field of accelerator physics [28], it was first pointed out in the context of Stark deceleration in reference [26]. The result can be seen in the left column of Figure 3, where the longitudinal phase space of OH packets is shown versus increasing phase angle. In Figure 3, the dark lines represent the separatrix, partitioning stable deceleration phase space from that of unstable motion as calculated from equation (2) in reference [20]. Each dot represents the position in phase space of a simulated molecule. In the absence of coupling between the longitudinal and transverse motions, one would expect the entire area inside the separatrix to be occupied. Therefore, the structure in these graphs is evidence of the importance of the transverse motion. The S parameter labeling each column of Figure 3 was previously defined in references [26,30]. $S = 1$ refers to a standard deceleration scheme in which stages are switched sequentially, while $S = 3, 5, 7...$ denote "overtone" sequences in which the molecules traverse $S - 2$ charged stages before fields are switched.

In the left column of Figure 3, the coupling of longitudinal and transverse motions is responsible for two effects[2]: first, in the center of the stable area at $\phi_0 = 0°$ — near the synchronous molecule — the density of stable molecules is less than in the surrounding area. This is because molecules that oscillate very near the synchronous molecule experience little transverse guiding [26]. This effect is not dramatic and is only discernable for an exceedingly large number of stages. Furthermore, this effect is even less important for the increased phase angles typically used for deceleration, since for these switching

sequences the synchronous molecule experiences more of the transverse guiding forces than it does during bunching. The second effect, which is much more evident, is the absence of molecules at intermediate distances from the synchronous molecule as shown in the left column of Figure 3. This so-called 'halo' is due to parametric amplification of the transverse motion and is similar to the effects seen in cold molecule storage rings [27] as well as charged particle accelerators [29]. Essentially, the longitudinal oscillation frequency of a molecule in this region is matched to the transverse oscillation frequency, leading to amplification of the transverse and longitudinal motion and consequent loss [26].

There is a compromise between decreasing longitudinal phase-space area and increasing transverse guidance for increasing ϕ_0. To demonstrate this effect, we decelerate molecules to a fixed v_{final} and vary the phase angle used to reach this velocity. This is done either by changing the voltage applied to the decelerator rods or by modifying the effective length of the decelerator itself for each ϕ_0 of interest. The experimental data shown in Figure 4 is the result of varying the voltage applied to our decelerator rods (squares) and the effective decelerator length (circles). Both lowering the decelerator voltage and using shorter lengths of the decelerator for slowing requires increasing ϕ_0 to observe the same v_{final} of 50 m/s. We are able to effectively shorten the decelerator by initially bunching the packet for a given number of stages before beginning a slowing sequence. Note that we use $S = 3$ bunching to remove any transverse/longitudinal couplings during these first stages, then switch back to $S = 1$ slowing for the remainder of the decelerator. The phase stable region of $S = 1$ for $\phi_0 \geq 40°$ is entirely contained within that of $S = 3$ at $\phi_0 = 0°$, therefore no artifacts from initial velocity filtering are present in this data. We observe that, contrary to the predictions of the one-dimensional

---

[2] For these phase space simulations, the input molecular beam has longitudinal spatial and velocity distributions that overfill the acceptance area.
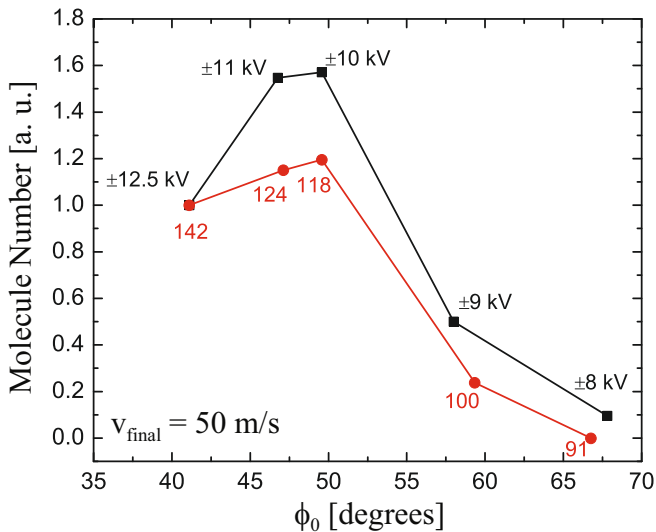
Fig. 4. (Color online) Experimental results from changing the voltage on decelerator rods (squares) and decreasing the effective decelerator length (circles). Effective slower length is modified by initially operating the decelerator at $\phi_0 = 0°$, $S = 3$, then slowing with $S = 1$ to $v_{final} = 50$ m/s for the number of stages labeled. Both curves illustrate that transverse/longitudinal couplings are strongly dependent on phase angle, and have a marked effect on decelerator efficiency.

theory [20], a higher phase angle can lead to greater decelerator efficiency up to some maximum ϕ_0. This is a direct consequence of distributed transverse/longitudinal couplings illustrated in Figure 3. At even larger phase angles, the longitudinal phase-space acceptance becomes a limiting factor. The labels next to each data point correspond to either the voltage applied to the decelerator rods (squares) or the number of utilized $S = 1$ slowing stages (circles). Figure 4 further illustrates that the transverse/longitudinal couplings outlined by reference [26] reduce decelerator efficiency, and are highly dependent on phase angle.

The coupling between longitudinal and transverse motion is detrimental to efficient operation of a Stark decelerator, reducing the total number of decelerated molecules. This effect will be even worse for decelerating molecules with an unfavorable Stark shift-to-mass ratio. Fortunately, the transverse and longitudinal motions can be decoupled by introducing a transverse focusing element to the deceleration beam line that overwhelms the transverse focusing provided by the deceleration electrodes in analogy to the focusing magnets of charged-beam machines. This technique also has the advantage of providing a larger stable region in the transverse phase space which further enhances the decelerated molecule number. The remainder of this manuscript discusses methods of implementing a transverse focusing element to decouple the longitudinal and transverse motion. We note that while $S = 3$ bunching has been previously discussed [26,30], the dynamics of decelerated packets under such operation have not been investigated. In Section 4 we discuss the effectiveness of $S = 3$ deceleration as well as other modified "overtone"

schemes. Section 5 presents an improved design for a Stark decelerator that solves this problem of distributed longitudinal and transverse loss and also reduces the previously described overfocusing losses at the final stage.

4 Decelerator overtones

The simplest method for introducing a transverse focusing element to the decelerator beam line is to let the molecules fly through an energized deceleration stage without removing the field. In this manner, molecules experience the transverse focusing of the entire stage without their longitudinal motion affected. Traditional longitudinal phase stability requires the switching of the fields to occur on an upward slope of the molecular potential energy, i.e., faster molecules are slowed more while slower molecules are slowed less than the synchronous molecule. Hence, it is necessary to de-sample the bunching switching rate by an odd factor (3, 5, 7...): the so-called decelerator overtones [30]. For convenience, we define the quantity $S = v_0/v_{Switch}$, where v_0 is the synchronous molecule velocity and the switching speed v_{Switch} is given as the stage spacing L divided by the switching time-interval. Reference [30] considered only the bunching case. In this work, we generalize to the case of actual deceleration. However, the above definition of S is still valid. That is, S is constant despite the fact that both v_0 and v_{Switch} vary when $\phi_0 > 0°$. With this definition we see that traditional deceleration can be described by $S = 1$, while the method of de-sampling the switch rate by a factor 3 is described by $S = 3$. These two methods of deceleration can be seen in Figures 5b and 5c, where their respective switching schemes are shown for $\phi_0 = 0°$. By switching at one-third the rate, the molecule packet flies through a deceleration stage that is energized and experiences enhanced transverse guiding.

Longitudinal phase space simulations of $S = 3$ slowing at various phase angles are shown in the right column of Figure 3. No structure is present in these plots. Also, the region of longitudinal phase stability for $S = 3$ — even at $\phi_0 = 0°$ — is reduced compared to $S = 1$. This is because the maximum stable velocity, as calculated from equations (2) and (6) of reference [20], depends on the spacing between deceleration stages as $L^{-1/2}$, and thus, the separatrix velocity bound is reduced by a factor of $\sqrt{3}$[3]. Nonetheless, the absence of coupling to the transverse motion leads to a larger number of molecules for the $\phi_0 = 0°$ case shown in the uppermost panel of Figure 3. In a given decelerator, $S = 3$ slowing requires a factor of three higher phase angle than $S = 1$ to reach the same final velocity. As illustrated in Figure 3, this fact severely limits the practicality of $S = 3$ as a deceleration scheme, as it implies a dramatic reduction in velocity acceptance at the highest phase angles.

---

[3] Physically, this is because the molecules fly longer between deceleration stages, and thus, the velocity mismatch can lead to a larger accumulation of spatial mismatch.
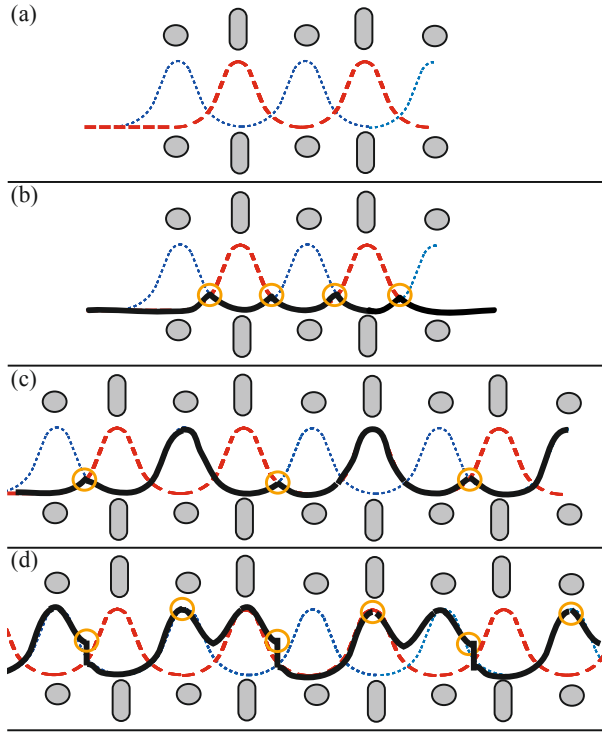
Fig. 5. (Color online) Deceleration schemes. (a) Potential energy shift of polar molecules in the Stark decelerator. The dotted (blue) curves show the potential energy shift when the horizontal (circular cross section) electrodes are energized, while the dashed (red) curves show the potential energy shift when the vertical (elongated cross section) electrodes are energized. Deceleration proceeds by switching between the two sets of energized electrodes. In panels (b)–(d), the thick black line indicates the potential experienced by the molecules. The empty circles indicate a switching event. (b) Traditional ($S = 1$) operation at $\phi_0 = 0°$. For phase stability, the switching always occurs when the molecules are on an upward slope, and as such the molecules are never between a pair of energized electrodes. Thus, the maximum transverse guiding is never realized. (c) First overtone operation ($S = 3$) at $\phi_0 = 0°$. By switching at one-third of the $S = 1$ rate, the molecules are allowed to fly directly between an energized electrode pair, and thus, experience enhanced transverse guiding. (d) Optimized first overtone operation ($S = 3+$) at $\phi_0 = 0°$: initially, the packet rises the Stark potential created by one set of electrodes. When the molecules reach the apex of this potential, the alternate set of electrodes is energized in addition. In this way, the molecules experience one more stage of maximum transverse guiding for each slowing stage. Note that, to minimize the un-bunching effect, the grounded-set of electrodes is switched on when the molecules are directly between the energized electrodes.
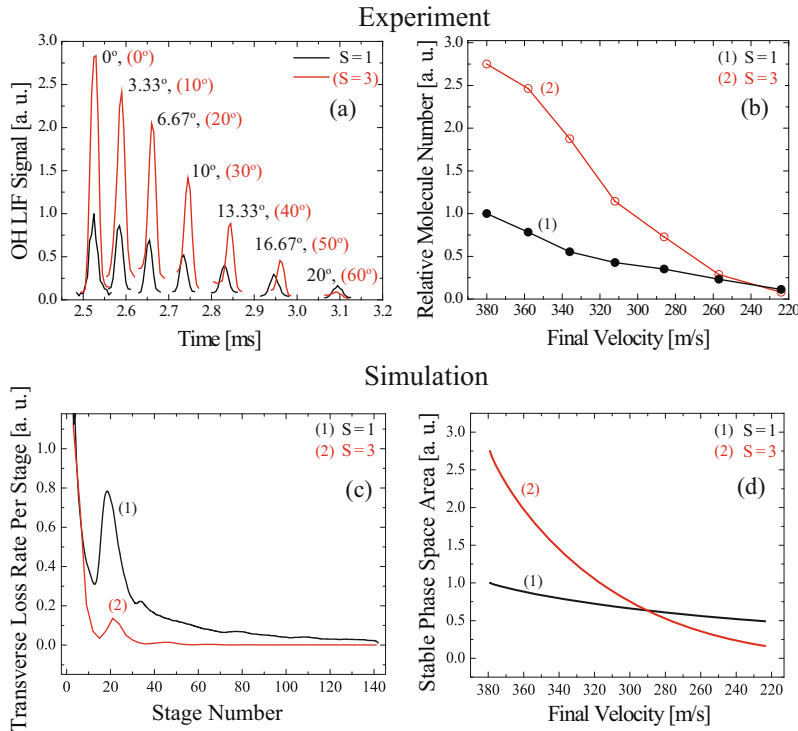
Fig. 6. (Color online) Comparison of deceleration using $S = 3$ versus $S = 1$. (a) Experimental ToF data of decelerated OH packets with $S = 3$ (top) and $S = 1$ (bottom). Note the factor of three between $S = 1$ and $S = 3$ phase angles. (b) Deconvolved, integrated molecule number for $S = 3$ (trace 2) and $S = 1$ (trace 1) for the packets shown in panel (a). (c) Simulated transverse loss rate per stage for $S = 1$ (trace 1) and $S = 3$ (trace 2) deceleration. As expected, $S = 1$ results in larger transverse loss rates throughout. (d) Calculated stable longitudinal phase-space area for $S = 1$ (trace 1) and $S = 3$ (trace 2), with initial points scaled to the experimental ratio of 2.75. The above panels highlight that the observed shortcoming of $S = 3$ deceleration is entirely due to loss of longitudinal velocity acceptance at high phase angles.

Shown in Figure 6a are experimental decelerated molecular packets for $S = 3$ (upper) and $S = 1$ (lower) versus increasing phase angle. For each successive packet, the $S = 3$ phase angle increases by $10°$ in the range $\phi_0 = 0–60°$, while the $S = 1$ phase angle increases by $10°/3$. In this manner, the packets are decelerated to roughly the same velocity. There is a slight difference at the highest phase angles shown because the total number of stages in our decelerator (142) is not an exact multiple of 3. In Figure 6b the de-convolved total molecule number for each of these packets is plotted versus final speed. While the $S = 3$ method dominates over $S = 1$ for small phase angles, its effectiveness decreases as the deceleration becomes more aggressive — by 224 m/s, the
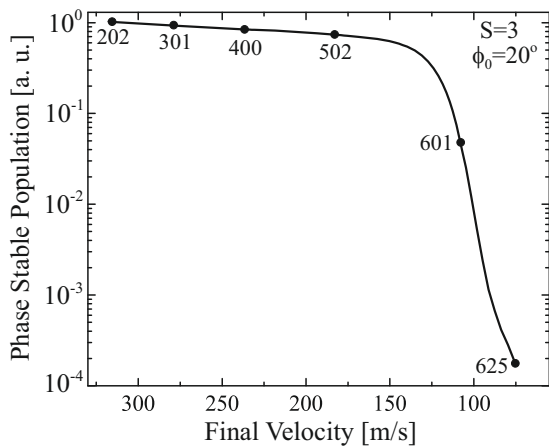
Fig. 7. Monte Carlo results for decelerated molecule number using $S = 3$ and $\phi_0 = 20°$ versus final velocity. The number next to each data point is the number of stages used. Because of transverse overfocusing and longitudinal velocity filtering, essentially no molecules survive below 100 m/s.

$S = 1$ molecule number is already larger than that of $S = 3$. This behavior is expected since the phase angle used to decelerate to 224 m/s is 60°, while the required $S = 1$ phase angle is only 20°. Although the $S = 3$ longitudinal phase bucket does not exhibit structure, it is so much smaller in enclosed area than the $S = 1$ that its total molecule number is smaller. The simulation results of Figure 6c and the theory results of Figure 6d support this description. Figure 6c shows that, even at $\phi_0 = 80°$, the transverse loss rate per stage is at all times greater for $S = 1$ than $S = 3$. However, the calculated longitudinal phase-space acceptance of Figure 6d mirrors the behavior observed experimentally in Figure 6b when the initial points are scaled to the experimental ratio of 2.75. This scaling accounts for the aforementioned 'halo' in the slowed $S = 1$ packet, which persists relatively unchanged over the range of $S = 1$ phase angles used ($\phi_0 = 0$–$20°$). The fact that the theory curves of Figure 6d cross at a higher velocity than the data of Figure 6b suggests there is increased transverse guiding of $S = 3$ slowing at high phase angles. Nevertheless, even with 142 stages of deceleration, $S = 3$ is unfavorable for velocities below 224 m/s due to reduced stable phase-space area. The peak in the loss rate observed in Figure 6c at ~20 stages is due to loss of quasi-stable molecules near the beginning of the deceleration sequence and is not observed beyond 40 stages.

At this point, one would expect that operation at lower phase angles would permit realization of the gain produced by the $S = 3$ method. This can be accomplished by naively using a longer decelerator. A simulation of this kind is presented in Figure 7, which plots the number of molecules present after deceleration at $\phi_0 = 20°$ versus final velocity[4]. The number next to a data point represents the number of deceleration stages used. Initially the decelerated molecule number is relatively flat versus fi-

nal velocity. However, after about 500 stages (180 m/s), the number of decelerated molecules begins to decrease and dramatically falls off after 550 stages (150 m/s). Very few molecules survive below 100 m/s. This is because for $S = 3$ the decelerated molecules must fly through an entire stage while experiencing a guiding force in only one dimension (see Fig. 5c). Once the molecules are at slower speeds they can spread out in one transverse dimension or be over-focused in the other and collide with the rods. As the mean kinetic energy of the slowed packet becomes comparable to the full potential height, the packet can be nearly stopped as it traverses the intermediate charged stage. This has two consequences: (1) longer transit time leading to more intense transverse focusing; and (2) velocity filtering of the low-speed packet as slower molecules are longitudinally reflected from this potential.

The transverse loss responsible for the extreme drop in molecule number for $S = 3$ deceleration also occurs in traditional deceleration, but to a lesser degree. Because of this decrease in molecule number at low speeds, the usefulness of slowing with $S = 3$ is generally limited to experiments that do not require the lowest velocities, such as microwave spectroscopy and collision experiments [31–33]. We note also that our simulations predict no low-velocity gain when using slowing sequences containing combinations of deceleration at $S = 1$ and bunching at $S = 3$.

A natural extension of the above overtone deceleration is the use of what we have termed a "modified decelerator overtone", denoted by an additional plus sign, i.e., $S = 3+$. Deceleration in this manner is shown in Figure 5d for $\phi_0 = 0°$. In this method, deceleration proceeds similarly to conventional $S = 3$. However, $S = 3+$ sequences yield confinement of the packet in both transverse dimensions. This is achieved by charging all slower rods for the period in which the synchronous molecule is between switching stages. In order to minimally disrupt the longitudinal dynamics of the synchronous molecule, the second set of slower rods is charged only when the molecule is at the peak of the longitudinal potential from the first rod set. The packet then traverses two charged rod pairs before reaching the next switching stage, at which point the rod pair that was originally charged is grounded. While this does create a slight anti-bunching effect, i.e., molecules in front of the synchronous molecule gain a small amount of energy, it provides an extra stage of transverse guidance in comparison to $S = 3$. Experimental results of this method of slowing are shown in Figure 8 for comparison to deceleration using both $S = 1$ and $S = 3$. Figure 8a displays a unique consequence of the $S = 3+$ switching sequence, where operation at $\phi_0 = 0°$ leads to deceleration. Figure 8b shows that operation with $S = 3+$ provides slightly more molecules than $S = 3$, but the loss of molecules due to decreased longitudinal velocity acceptance remains a problem. The increase in molecule number for $S = 3+$ over $S = 3$ is due to the extra stage of transverse guidance, which for the higher-velocity packets we measured leads to a larger transverse acceptance.

---

[4] In this simulation, $\phi_0 = 20°$ is chosen because it produces the most gain over $S = 1$ in our deceleration experiments.
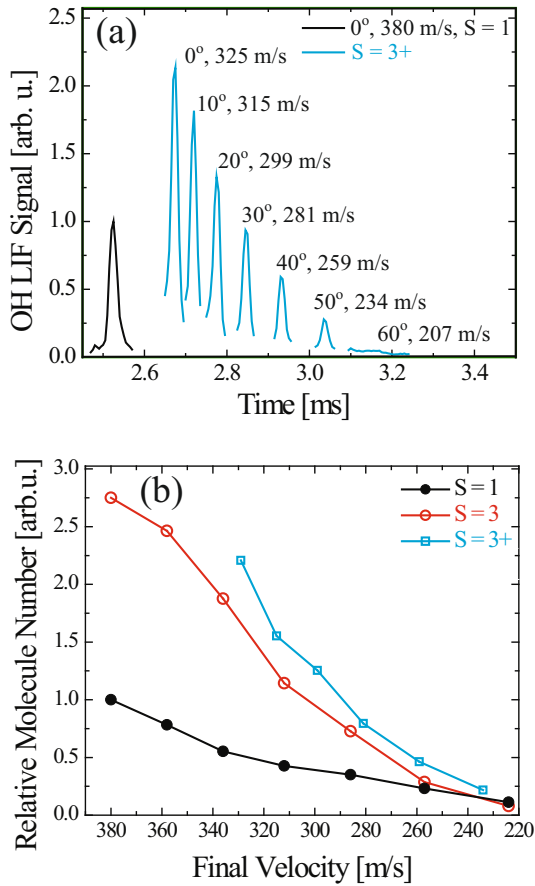
Fig. 8. (Color online) (a) Experimental ToF data of decelerated OH packets produced using the $S = 3+$ modified overtone. Also shown for comparison is the experimental bunching packet for operation at $S = 1$. (b) The de-convolved, integrated molecule number calculated from $S = 3+$ (open squares), $S = 3$ (open circles), and $S = 1$ (dots) data.

To determine whether the extra stage of transverse guidance would counter the overfocusing effects[5], we perform simulations of $S = 3+$ deceleration at $\phi_0 = 20°$ for a varying number of deceleration stages. The results of these simulations, shown in Figure 9, are similar to the results for $S = 3$. Namely, as the decelerator length is increased and the molecules' speed is reduced, there is a marked molecule number loss for velocities below 200 m/s. In our simulations, we could not observe any molecules below 100 m/s. Again, transverse overfocusing and longitudinal filtering of the molecular packet by the deceleration electrodes are responsible for large losses in the decelerator, and this suggests that measures beyond modified switching schemes are required to overcome these loss mechanisms.

---

[5] While this may seem counterintuitive, in some cases when the transverse overfocusing is not too strong, the addition of another focusing element can change the sign of the molecules transverse velocity, keeping the beam confined within the decelerator.
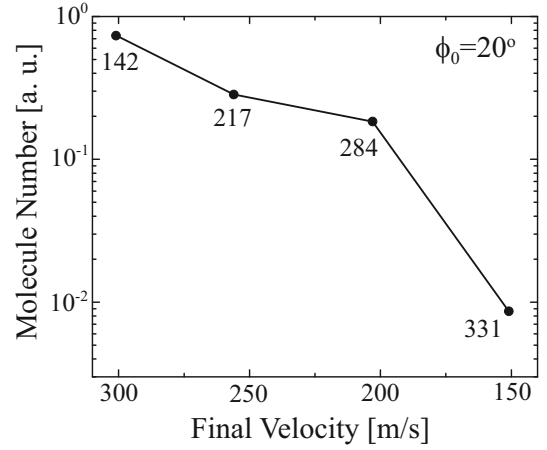
Fig. 9. Monte Carlo results of decelerated molecule number using $S = 3+$ and $\phi_0 = 20°$ versus final velocity. The number next to each data point is the number of stages used. Because of transverse overfocusing, essentially no molecules survive below 100 m/s.

5 Quadrupole-guiding decelerator

In addition to modifying the timing sequences of existing decelerators, it is possible, and perhaps preferable, to uncouple the longitudinal motion inside the Stark decelerator from the transverse motion by redesigning the decelerator electrode geometry. One simple redesign, which we call the quadrupole-guiding decelerator (QGD), is shown in Figure 10a. In this decelerator, a quadrupole-guiding stage (Fig. 10b) is interleaved between each deceleration stage. While it may not be necessary to have a quadrupole-guiding stage between each deceleration stage (especially in the beginning of the decelerator), it simplifies the analysis and will be used here. The switching of the electric fields inside a QGD is similar to a traditional decelerator operated with $S = 1$. Figure 10c shows the potential energy experienced by a molecule decelerated at $\phi_0 \approx 45°$ and is represented by a thick black curve. In this panel, the quadrupole-guiding electrodes are omitted for clarity. Note that the quadrupoles are always energized and their center coincides with the $\phi_0 = 0°$ position, while $\phi_0 = 90°$ occurs between the deceleration electrodes.

Deceleration with a QGD enjoys the same longitudinal phase-stability as a traditional decelerator. In a QGD, the maximum stable excursion position $\Delta\phi_{max}$ and velocity Δv_{max} will differ from that of the traditional decelerator because the decelerating electrodes are most likely further apart. In other words, to prevent high-voltage breakdown, the quadrupole stages require the same inter-stage spacing as deceleration stages in a traditional decelerator. Thus, the decelerating electrodes for a QGD will be twice as far apart as in our traditional decelerator, which possesses an inter-stage spacing of 5.5 mm. Since the dependence of the decelerating force on ϕ_0 is less steep, the shape of the stable longitudinal phase space will change. Understanding the shape of the stable longitudinal phase area is crucial for predicting the performance of the QGD, and can be derived by examining the longitudinal forces inside the
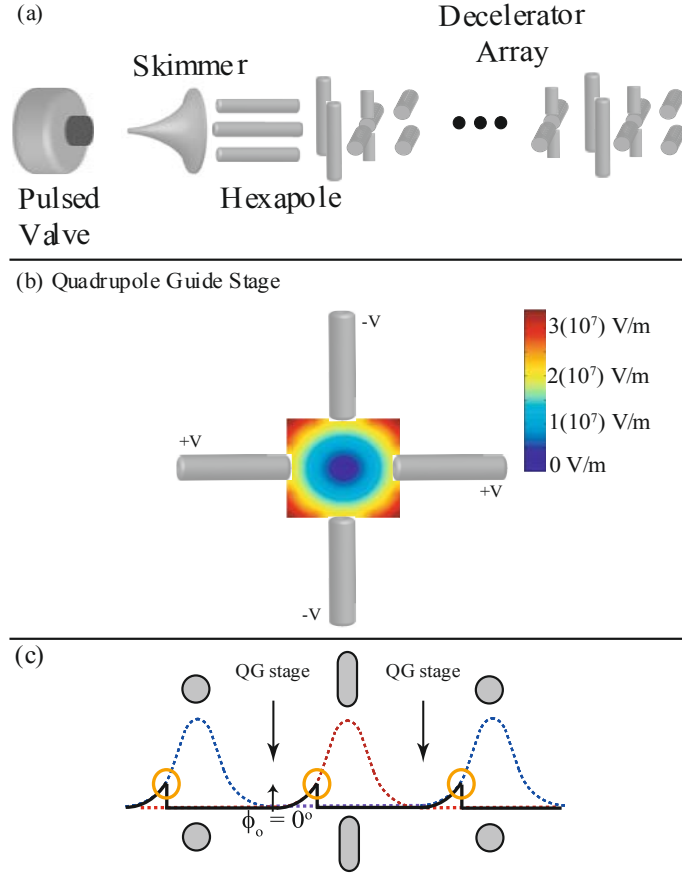
Fig. 10. (Color online) Quadrupole-guiding decelerator. (a) Schematic of QGD. (b) Electric field of quadrupole guiding stage energized to ±12.5 kV. (c) Switching scheme for deceleration with the QGD.

QGD. Shown in Figure 11a is the on-axis Stark shift of an OH molecule in the $|2, \pm 2, -\rangle$ state inside the unit cell, defined as 3 deceleration stages of the QGD. The quadrupole rods are held at a constant ±12 kV for this calculation, though their contribution to the longitudinal potential is negligible. The solid line is the Stark shift due to the slowing stage centered at 11 mm, while the dashed line is the Stark shift of the stages which will be energized when the fields are switched. The subtraction of these two curves, shown in Figure 11b as a solid line, is the amount of energy removed each time the fields are switched, ΔKE. We represent ΔKE as sum of sine-functions [30]

$$\Delta KE(\phi) = \sum_{n=odd} a_n \sin(n\phi), \quad (1)$$

where we have used the definition of the phase angle $\phi = (z/L)180°$. A fit of the first three terms of this equation to the actual ΔKE for deceleration stages spaced by 11 mm is shown as a dashed line in Figure 11, resulting in the fit values $a_1 = 1.221$ cm^{-1}, $a_3 = 0.450$ cm^{-1}, and $a_5 = 0.089$ cm^{-1}. Using this fit, we derive the equation of motion of the molecules about the synchronous molecule position as

$$\frac{d^2\Delta\phi}{dt^2} + \frac{\pi}{mL^2}(\Delta KE(\Delta\phi + \phi_0) - \Delta KE(\phi_0)) = 0, \quad (2)$$

where we have used the excursion of the molecule from the synchronous molecule $\Delta\phi = \phi - \phi_0$. The maximum stable forward excursion of a non-synchronous molecule is exactly the same as a traditional decelerator and is given as [20]

$$\Delta\phi_{max}^+(\phi_0) = 180° - 2\phi_0. \quad (3)$$

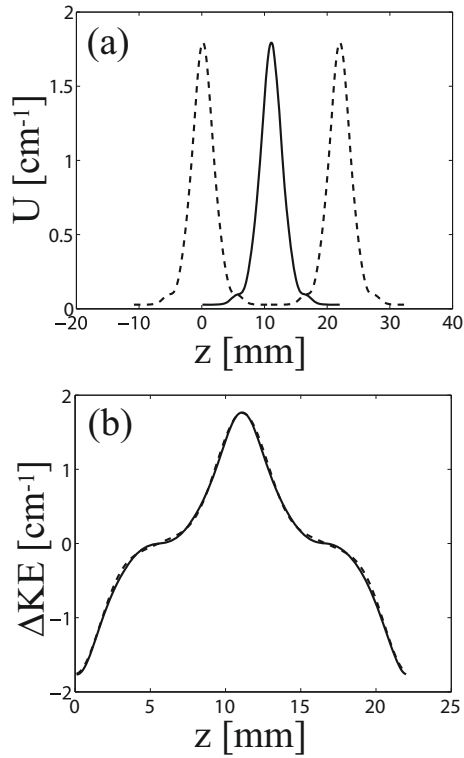We calculate the work done in bringing a molecule starting at this position with zero velocity to the synchronous molecule position as

$$W(\phi_0) = \int_{Start}^{End} F dx$$
$$= -\frac{1}{\pi} \int_{\Delta\phi_{max}^+(\phi_0)}^{0} \sum_{n=odds} (a_n[\sin(n(\Delta\phi + \phi_0)) - \sin(n\phi_0)]) d(\Delta\phi). \quad (4)$$

Integrating this equation and setting it equal to the kinetic energy yields the maximum stable excursion velocity:

$$\Delta v_{max}(\phi_0) =$$
$$2\sqrt{\sum_{n=odds} \frac{a_n}{m\pi} \left(\frac{\cos(n\phi_0)}{n} - (\frac{\pi}{2} - \phi_0)\sin(\phi_0) \right)}, \quad (5)$$
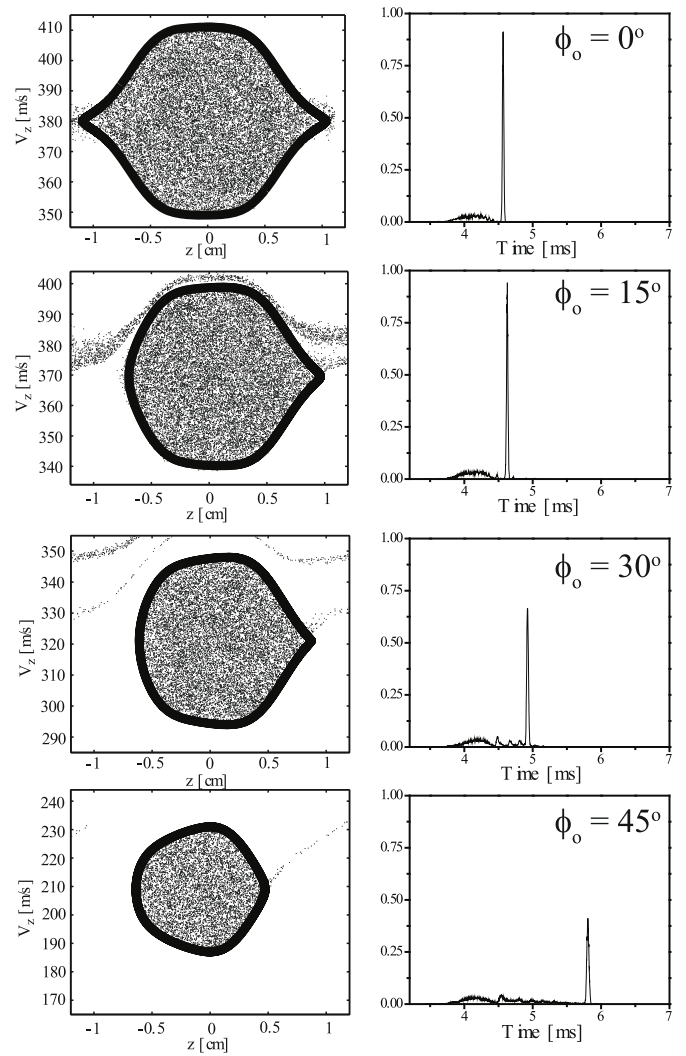
where ϕ_0 is now in radians.

Fig. 11. (a) The Stark shift of an OH molecule in the $|2, \pm2, -\rangle$ state inside the QGD. The solid curve is the Stark shift due to the slowing electrodes, while the dashed curve is the Stark shift due to the electrodes that will be energized at the switching time. (b) The change in the molecule's kinetic energy as a function of position is shown (solid) as well as a fit of equation (1), including up to n = 3 (dashed). The solid curve is calculated from the subtraction of the two curves in panel (a).

Fig. 12. The left column is stable phase space of molecules decelerated inside the QGD. The solid line is the separatrix predicted by the theory, while the points represent positions of molecule in the 3D Monte Carlo simulations. The right column shows the ToF spectra of OH molecules in the $|2\pm2, -\rangle$ state at the exit of this decelerator which has 142 deceleration stages, along with 142 quadrupole stages.
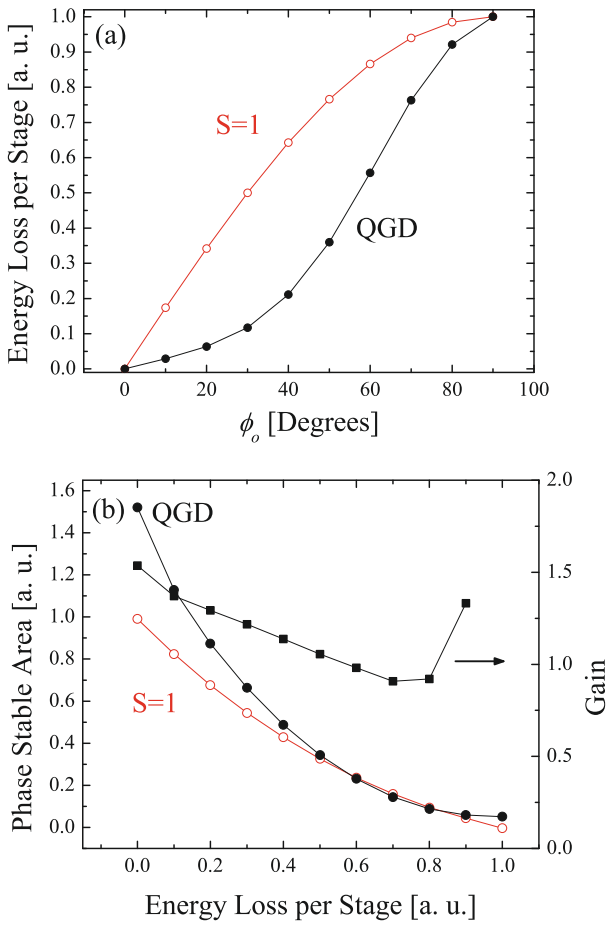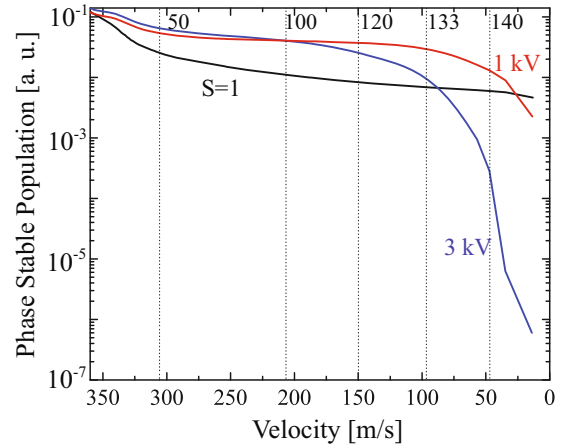
Using equations (2–5) it is possible to solve for the longitudinal separatrix, which separates stable deceleration from unstable motion inside the decelerator. These separatrices are shown (thick black lines) along with the results of Monte Carlo simulations of a QGD in the left column of Figure 12 for successive phase angles. The longitudinal phase space is shown with each dot representing the position of a stable molecule. The lack of structure inside these separatrices is evidence of the lack of coupling between the transverse and longitudinal modes. The right column, which shows simulated ToF curves, reveals a single stable peak arriving at later times as ϕ_0 is increased. These simulations are for a single $|2, \pm2, -\rangle$ state of OH and do not exhibit the large background contribution of the other states of OH present in experimental ToF data.

From the comparison of the simulations with the analytical results represented by the separatrices, we see that the simple theory of equations (2–5) is quite accurate in describing the longitudinal performance of the QGD. Thus, by numerically integrating the area inside these separatrices, we can predict the longitudinal performance of the QGD relative to the traditional decelerator. As seen in Figure 13a, the energy removed per stage of the QGD

is smaller than that of a traditional decelerator for all $0° < \phi_0 < 90°$ because the decelerator stage spacing (in this simulation) is twice that of a traditional decelerator. For this reason, given the same number of deceleration stages, QGD deceleration with the same ϕ_0 as in a traditional decelerator leads to a faster beam. When comparing the longitudinal acceptance of the two types of decelerators it is important to take the limit of high phase angles where both values of ΔKE converge. Nonetheless, the longitudinal phase-space acceptance of the QGD shows some gain over that of traditional deceleration as shown in Figure 13b. This gain at a fixed energy loss per stage is primarily due to the increased physical size of the stable longitudinal phase space resulting from the larger deceleration stage spacing.

Fig. 14. (Color online) Simulations of the phase-stable molecule number as a function of stage number in the QGD and $S = 1$ decelerator. The voltage on the quadrupole stages of the QGD is held constant throughout the deceleration sequence. All simulation data is for $v_{final} = 14$ m/s. The traces shown are $S = 1$ deceleration at $\phi_0 = 30.43°$, QGD operated with ± 1 kV on the quadrupoles, and QGD operated with ± 3 kV on the quadrupoles. Note the decrease in stable molecule number in the last several stages for the QGD results. This decrease is due to transverse overfocusing of the slow molecules through the final few quadrupole stages, and suggests that scaling of quadrupole voltage is necessary.
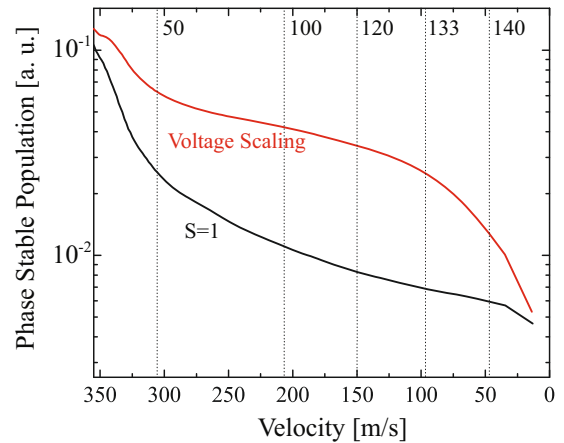
Fig. 13. (Color online) (a) The energy removed per stage as a function of phase angle for both traditional deceleration and deceleration with a QGD. Both curves are calculated for OH in the $|2, \pm 2, -\rangle$ state and scaled down by 1.76 cm^{-1} at $\phi_0 = 90°$. (b) The calculated longitudinal phase-stable area for deceleration versus energy loss per stage for traditional deceleration and deceleration with a QGD is plotted on the left axis. The gain of the QGD over traditional deceleration is plotted on the right axis. Note that for a given energy loss the gain in phase stable area due to the larger volume of the QGD is ≤ 1.5 for all $0° < \phi_0 < 80°$.

Since Figure 13 compares only the total area inside the separatrix — and $S = 1$ deceleration does not completely fill this area due to the coupling effects — this gain is actually an underestimate of the QGD longitudinal performance. Furthermore, these graphs do not include transverse focusing effects, which can only be properly included through detailed simulation. The results of Monte Carlo simulations including these transverse effects are shown in Figure 14. The number of decelerated molecules versus final speed is plotted for both the traditional decelerator operating at $S = 1$ and the QGD operating at two different quadrupole rod voltages, ± 1 kV and ± 3 kV. While the QGD initially delivers more molecules, once the molecules are decelerated below 100 m/s, the decelerated molecule number falls off abruptly. This behavior is expected since, for these simulations, the voltage on

Fig. 15. (Color online) Monte Carlo simulation results for the decelerated molecule number using traditional $S = 1$ deceleration ($\phi_0 = 30.43°$) and deceleration using a QGD ($\phi_0 = 52.75°$) with a dynamic voltage scaling of $(v/v_{initial})^{0.875}$. For both curves, 142 stages of deceleration were used, and $v_{final} = 14$ m/s. The different phase angles chosen for the two decelerators are a result of their differing potential profiles for deceleration. The vertical dashed lines represent the deceleration stage at the given velocity. Note that when the quadrupole voltage within the QGD is scaled in this manner, we observe a 40% gain in molecule number at 14 m/s, and a factor of 5 gain over $S = 1$ at higher velocities.

the quadrupole-guiding stages is held constant throughout the slowing sequence. As detailed in equation (3) of reference [19], the focal length of a transverse guiding element is directly proportional to the molecular kinetic energy. Therefore, as the mean speed of the packet is decreased, the molecules are overfocused and collide with the decelerator electrodes. This can be prevented by lowering the voltage on the quadrupole-guiding stages during the deceleration process. Figure 15 displays simulation results of deceleration with this dynamically scaled voltage compared to $S = 1$ slowing at $\phi_0 = 30.43°$. For this simulation, the quadrupole voltages are scaled by $(v/v_{initial})^{0.875}$ after each deceleration stage, where v is the instantaneous packet velocity directly following each stage switch. The exponent of 0.875 is found empirically to produce the most gain at $v_{final} = 14$ m/s. For ease of simulation, the transverse forces are scaled by $(v/v_{initial})^{0.875}$ whenever the molecules are closer to a quadrupole-guiding stage than to a deceleration stage. While this may be a poor approximation at the lowest speeds, it will likely lead to an underestimate of the decelerated molecule number since the transverse guidance of the quadrupole-guiding stage extends beyond this regime. Even if it leads to an overestimate, proper control of the quadrupole voltages may compensate any overfocusing introduced by the decelerating elements. As seen in Figure 15, dynamically controlling the voltage of the quadrupole-guiding stages leads to a factor of 5 increase in decelerated number for larger velocities (>80 m/s) and delivers about 40% more decelerated molecules than traditional $S = 1$ deceleration provides at the lowest final speeds (14 m/s). Because the voltages applied to the quadrupole-guiding stages are relatively low, dynamic control of them should be possible using an analog waveform generator and high-voltage amplifier. It should be noted that the optimal voltage scaling may vary among decelerators since the real focal length depends sensitively on the electrode construction, and at low speeds the transverse focusing of the decelerator electrodes becomes significant. This is, presumably, because the overfocusing of the decelerator electrodes can be compensated to a certain degree by injecting molecules which are already slightly overfocused. In other words, two focusing stages can overcome the overfocusing of a single stage. Thus, it may be possible to use adaptive algorithms to optimize the quadrupole voltage or change the design of the decelerating electrodes so that they provide less transverse focusing, and maximize the number of decelerated molecules beyond what is reported here [33].

One important advantage of the QGD over traditional decelerators is its inherent ability to support more deceleration stages. Because the molecules experience a tunable transverse focusing element after each deceleration stage, there is little loss in efficiency by extending the number of deceleration stages. In fact, as seen in Figure 16, there is essentially no loss until the molecules are decelerated to the lowest speeds previously discussed. This low-velocity loss is due to the aforementioned transverse overfocusing and longitudinal reflection. The former loss mechanism may be overcome, while the latter presents a fundamen-
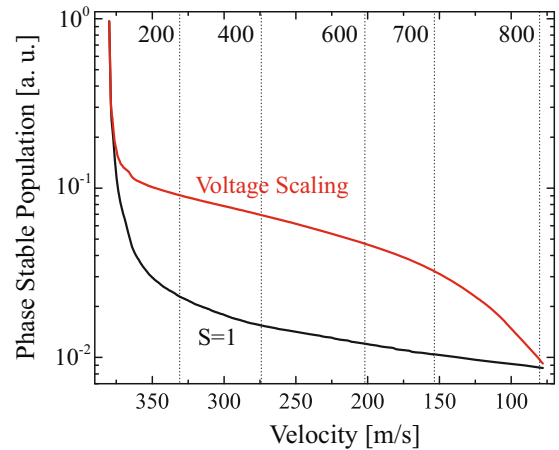
Fig. 16. (Color online) $S = 1$ simulation results for $v_{final} = 80$ m/s ($\phi_0 = 5.22°$) plotted along with simulation results using the voltage-scaled QGD to the same v_{final} ($\phi_0 = 23.5°$). The number labeling each vertical dashed line is the number of deceleration stages necessary to reach the given velocity. Note the large number of stages (803) used to reach 80 m/s, which suggests that a very long QGD may be employed for slowing molecules with a poor Stark shift to mass ratio.

tal limit. Even with this loss, the QGD outperforms both $S = 3$ (Fig. 7) and $S = 3+$ (Fig. 9). Thus, the QGD is an ideal decelerator for more efficiently producing cold molecules and, perhaps more importantly, the ideal decelerator for slowing molecules with poor Stark shift to mass ratios, like H_2O and SO_2.

6 Conclusion

In summary, we identify two specific loss mechanisms — transverse over-focusing and longitudinal reflection — observed in the operation of Stark decelerators and perform initial experiments and detailed Monte Carlo simulations to address them. While the use of decelerator overtones yields improvement over $S = 1$ deceleration at high to intermediate speeds ($v_{final} > 80$ m/s), the loss at very low velocities remains problematic. The QGD solves the problem of coupling between the transverse and longitudinal motions inside a Stark decelerator by introducing independent transverse focusing elements. By dynamically controlling the focal length (voltage) of these guiding elements, large improvements (factor of 5) in deceleration efficiency can be achieved for $v_{final} > 80$ m/s, which would prove useful for molecule collision studies [34]. Gains of 2 and 40% are also predicted for $v_{final} = 50$ m/s and 14 m/s, respectively. Electrostatic [21] and magneto-electrostatic [25] trapping experiments stand to benefit from such gain for $v_{final} \leq 50$ m/s. Furthermore, it appears that with dynamic control of the guiding stage focal length there should be no limit to the length of decelerator that can be built. This enables the deceleration of molecules with a poor Stark shift to mass ratio. However, we note that none of the techniques described in this article mitigate the longitudinal low-velocity loss due to

reflection, which appears to be a fundamental component of Stark deceleration. Building upon the strong correlation between simulation and experimental results, we are confident that the simulations presented in this work provide a solid guideline for future implementations of Stark deceleration.

References

1. A.V. Avdeenkov, J.L. Bohn, Phys. Rev. A **66**, 052718 (2002)
2. E.R. Hudson et al., Phys. Rev. A **66**, 063404 (2006)
3. D. DeMille, Phys. Rev. Lett. **88**, 067901 (2002)
4. J.D. Weinstein, R. deCarvalho, T. Guillet, B. Friedrich, J.M. Doyle, Nature **395**, 148 (1998)
5. K.M. Jones et al., Rev. Mod. Phys. **78**, 483 (2006)
6. J.M. Sage, S. Sainis, T. Bergeman, D. Demille, Phys. Rev. Lett. **94**, 203001 (2005)
7. D. Wang et al., Phys. Rev. Lett. **93**, 243005 (2004)
8. C. Ospelkaus et al., Phys. Rev. Lett. **97**, 120402 (2006)
9. H.L. Bethlem, G. Berden, G. Meijer, Phys. Rev. Lett. **83**, 1558 (1999)
10. S. Hoekstra et al., Phys. Rev. A **76**, 063408 (2007)
11. J.J. Gilijamse et al., J. Chem. Phys. **127**, 22102 (2007)
12. W.C. Campbell et al., Phys. Rev. Lett. **98**, 213001 (2007)
13. O. Bucicov et al., Eur. Phys. J. D **46**, 463 (2008)
14. A. Pe'er et al., Phys. Rev. Lett. **98**, 113004 (2007)
15. *Atomic and Molecular Beam Methods*, edited by G. Scoles (Oxford University Press, New York, 1988)
16. S.Y.T. van de Meerakker, private communication
17. H.L. Bethlem, G. Berden, F.M.H. Crompvoets, R.T. Jongma, A.J.A. van Roij, G. Meijer, Nature **406**, 491 (2000)
18. J.R. Bochinski et al., Phys. Rev. Lett. **91**, 243001 (2003)
19. J.R. Bochinski et al., Phys. Rev. A **70**, 043410 (2004)
20. E.R. Hudson et al., Eur. Phys. J. D **31**, 351 (2004)
21. S.Y.T. van de Meerakker et al., Phys. Rev. Lett. **94**, 023004 (2005)
22. M.R. Tarbutt, H.L. Bethlem, J.J. Hudson, V.L. Ryabov, V.A. Ryzhov, B.E. Sauer, G. Meijer, E.A. Hinds, Phys. Rev. Lett. **92**, 173002 (2004)
23. S.Y.T. van de Meerakker et al., J. Phys. B **39**, S1077 (2006)
24. S. Jung, G. Tiemann, C. Lisdat, Phys. Rev. A **74**, 040701(R) (2006)
25. B.C. Sawyer et al., Phys. Rev. Lett. **98**, 253002 (2007)
26. S.Y.T. van de Meerakker, N. Vanhaecke, H.L. Bethlem, G. Meijer, Phys. Rev. A **73**, 023401 (2006)
27. F.M.H. Crompvoets, H.L. Bethlem, J. Kupper, A.J.A. van Roij, G. Meijer, Phys. Rev. A **69**, 063406 (2004)
28. H. Wiedemann, *Particle Accelerator Physics I: Basic Principles and Linear Beam Dynamics*, 2nd edn. (Springer, Berlin, 2004)
29. T. Suzuki, Particle Accelerators **18**, 115 (1985)
30. S.Y.T. van de Meerakker, N. Vanhaecke, H.L. Bethlem, G. Meijer, Phys. Rev. A **71**, 053409 (2005)
31. E.R. Hudson et al., Phys. Rev. Lett. **96**, 143004 (2006)
32. B.L. Lev et al., Phys. Rev. A **74**, 061402(R) (2006)
33. J.J. Gilijamse et al., Phys. Rev. A **73**, 063410 (2006)
34. J.J. Gilijamse et al., Science **313**, 1617 (2006)